

NATURAL SCIENCE

Impacts of *Hymenolepis diminuta* (benign helminth worm) colonization on chronic pain and the central nervous system in Sprague Dawley rats

Haley Lippman

The following is an excerpt from a longer piece. For full text, please visit https://scholar.colorado.edu/concern/undergraduate_honors_theses/8s45q932q

Abstract

Over the last century, members of post-industrial societies have experienced a significant depletion of gut microbiota in terms of parasitic “old friends.” Consequently, the ability of the remaining microbiota to modulate immune responses has been drastically limited. Reduced immunoregulation causes the immune system to be overactive due to an improper balance between T helper 1 (Th1) and T helper 2 (Th2) immunity. Th1 immunity is used to fight intracellular pathogens, and it is mediated by inflammatory effector T cells. Th2 immunity fights extracellular pathogens through a humoral response that upregulates antibody production. It has been demonstrated that intestinal helminth worms, such as *Hymenolepis diminuta*, are responsible for a shift away from Th1 cell immunity and towards Th2 cell immunity, which promotes an anti-inflammatory phenotype through suppression of inflammatory effector T cells. A helminth-induced anti-inflammatory shift could potentially be used to counteract inflammatory disorders such as chronic neuropathic pain. Neuropathic pain is responsible for an upregulation of pro-inflammatory cytokines and a shift toward Th1 immunity. This study explored the use of helminthic therapy as a

treatment for neuropathic pain in the periphery and both neuropathic pain and cognitive dysfunction in the central nervous system through increased immune regulation.

We investigated the effects of *H. diminuta* on neuropathic pain development and cognition in male Sprague Dawley rats following chronic constriction injury of the sciatic nerve. Rats were colonized with *Hymenolepid diminuta* cystercercoids (HDCs; larval stage) prior to CCI surgeries. Von Frey testing measured levels of mechanical allodynia, Pavlovian fear conditioning measured declarative memory, and juvenile social exploration measured levels of anxiety. Inconsistent results from Von Frey and fear conditioning suggest that helminth worm therapy most likely does not improve mechanical allodynia or hippocampal-dependent learning and memory cognition. Neither CCI surgery nor helminth colonization impacted anxiety levels. Additionally, impacts of *H. diminuta* on molecular regulation of cytokine levels in the hippocampus were assessed using qRT-PCR. Hippocampus analysis demonstrated a shift toward an anti-inflammatory cytokine milieu following helminth treatment. These studies indicate that, although helminths did not consistently

impact behavior following CCI surgeries, *H. diminuta* therapy is a promising treatment for neuroinflammation in the brain.

Introduction

Chronic pain is a world-wide crisis that impacts more than 50 million people in the United States alone, and it has been connected to anxiety and depression, opioid addiction, and limited mobility (Dahlhamer, 2018). Because neuropathic pain has become an incredibly widespread issue, the neuroimmune causes of chronic pain are of great interest to the research community. [...]

According to the Center for Disease Control and Prevention, approximately 20% of the United States population is affected by chronic pain (Cragg, 2018), and this may be due, in part, to overactive effector CD4⁺ T cells that are not being adequately suppressed by T_{reg} cells. The presence of certain beneficial microbiota within the gut microbiome have been linked to increased numbers of regulatory T cells (Hewitson), so it is possible that exposure to these specific microbiota could be a potential treatment for chronic pain. Though humans coevolved with these microorganisms, humans within post-industrialized countries no longer serve as hosts to many of these microorganisms. It has proposed that the use of antibiotics, clean water, and sterilized medical techniques have caused the gut microbiome of humans living in post-industrialized countries to become a hostile environment for many commensal microorganisms (Bilbo, Wray, Perkins, & Parker, 2011; Ege, 2017; A. H. Liu, 2015; Villeneuve et al., 2018). This decreased microbial diversity correlates with decreased immunoregulatory functions of the host, and

the proposed link between these two factors is referred to as the hygiene hypothesis. More specifically, the hygiene hypothesis states that the depletion of microorganisms within the gut microbiome of a human can cause the immune system to be poorly educated, which in turn, can cause the immune system to be overactive in response to inappropriate stimuli. The positive correlation between the presence of microorganisms and improved immunoregulation can be supported on a molecular basis by the promotion of an anti-inflammatory phenotype of animals that host microorganisms.

An example of one of these microorganisms is *Mycobacterium vaccae* (*M. vaccae*). *M. vaccae* restores the immune balance between T helper 1 (Th1) and T helper 2 (Th2) responses. Th1 responses harness effector Th1 and Th17 cells to fight intracellular pathogens, and Th2 responses use antibody-mediated responses and suppression of inflammatory effector T cells to fight extracellular pathogens. *M. vaccae* modulates immunity of the infected animal by activating Th1-mediated responses and suppressing Th2 responses (Akkoc et al., 2008; Grange, Bottasso, Stanford, & Stanford, 2008; Hernández-Pando et al., 2008; Stanford, Stanford, & Grange, 2004; L. Zhang et al., 2016). This is the natural response of the body to attempt to attack and destroy the pathogen. [...]

Depending on the microorganism, upregulation of Th1 responses or upregulation of Th2 responses can be utilized to enhance immunoregulation and benefit host immunity, because both of these techniques can be used to restore the Th1/Th2 balance. For instance, parasitic microbes, such as helminth tapeworms, can regulate the immune

system by shifting the immunophenotype of their hosts from primarily mediating Th1 responses to facilitating Th2 responses (Villeneuve et al., 2018). Helminth tapeworms, called *Hymenolepis diminuta*, were used in this study because they are able to restore the Th1/Th2 balance of the host organism by promoting T_{reg} activation and effector CD4⁺ T cell suppression. These factors contribute to promoting an anti-inflammatory phenotype in the host. In addition to promoting immunoregulation, *H. diminuta* also avoid piercing the epithelial wall of the small intestines of their hosts, so they are considered benign helminths (Smyth et al., 2017). These two features make treatment with benign helminth parasites a very attractive research subject in regard to alleviating immunological disorders without causing tissue damage to the host.

[...]

In previous studies, *H. diminuta* have been proven to alleviate neuroinflammation, decrease cognitive disorders (Williamson et al., 2016), and decrease risks of autoimmune diseases (Fairweather & Cihakova, 2009). Additionally, the life cycle of *H. diminuta* offers a benefit that makes it an ideal candidate for the colonization of rats and mice in a laboratory setting. These helminths require a secondary, intermediate host for reproduction (Smyth et al., 2017; M. Zhang, Mathew, & Parker, 2018), which prevents these helminths from transmitting directly from rat to rat or from rat to human unintentionally. Common grain beetles can be used to allow *H. diminuta* eggs to mature into *Hymenolepis diminuta* cysticercoids (HDCs) that can be directly fed to rodents. The HDCs then colonize their hosts and grow into full helminth worms within the small intestines of the rodents. At this point,

the helminth worms produce eggs that are secreted in the fecal matter of the rodents; grain beetles eat the eggs, and the life cycle starts again (M. Zhang et al., 2018). The anti-inflammatory properties of *H. diminuta*, along with the benefits of laboratory use, make this species of helminth an ideal candidate for research in neuroinflammation and chronic pain.

This following set of experiments conducted are aimed at answering two questions concerning the effects of the introduction of the benign helminth worm *H. diminuta* into the gut microbiome of Sprague Dawley rats. The first goal of this experiment was to determine whether helminthic treatment was able to counteract the negative behavioral effects of a chronic constriction injury (CCI) on the left sciatic nerve of Sprague Dawley rats.

[...]

The second goal of this set of experiments, analysis of the hippocampus, showed a significant difference in the mRNA levels of several cytokines in rats that were colonized by *H. diminuta*. There was an increase of the anti-inflammatory cytokine, IL-10, along with a decrease in the IL-10 receptor. Additionally, there was a decrease in the expression of IL-13. Though this Th2-induced cytokine has been linked to several anti-inflammatory processes, it is also associated with allergen-induced asthma (Corren, 2013). Since treatment with *H. diminuta* causes an increase in immunoregulatory Th2 responses and a reduction in airway inflammation, this result was expected (McKenney et al., 2015). Colonization by *H. diminuta* generated an anti-inflammatory cytokine milieu within the hippocampus of Sprague Dawley rats, which suggests potential therapeutic uses for benign

helminthic treatment.

Methods

Subjects

Pathogen-free Sprague Dawley rats aged 10-12 weeks upon arrival were used for every experiment (Envigo). Rats were housed in pairs in Plexiglas cages with food and water available *ad libitum*. The Vivarium was temperature controlled at $23 \pm 3^\circ\text{C}$ and light-controlled with a 12 hour light-dark cycle. All methods were approved by the Institutional Animal Care and Use Committee of the University of Colorado Boulder.

[...]

Experiment 7: Analysis of Hippocampus mRNA

Hippocampus Extraction

Six weeks after colonization with *H. diminuta* eggs, rats were euthanized using i.p. 65 mg/kg sodium pentobarbital (Abbott Laboratories, North Chicago, IL, USA). Transcardial perfusion was performed using cold 0.9% saline. Following decapitation, the brain was removed, and the whole hippocampus was isolated. The hippocampus was flash frozen in liquid nitrogen and stored at -80°C .

Total RNA Extraction

The phenol:chloroform extraction method was used to isolate samples of total RNA from hippocampus tissue (Chomczynski & Sacchi, 1987).

[...]

cDNA synthesis

SuperScript II First Strand Synthesis System for RT-PCR (Invitrogen) was used to reverse transcribe total RNA into cDNA.

[...]

Quantitative Real-Time Polymerase Chain Reaction (qRT-PCR)

The Quantitect SYBR Green PCR Kit

(Quiagen, Valencia, CA) was used for PCR amplification of cDNA. Protocols for total RNA isolation, cDNA synthesis, and qRT-PCR can be found in previous publications (Frank, Fonken, Dolzani, et al., 2018).

[...]

Tissue Preparation and Bradford Assay

An extraction buffer solution (Invitrogen) and protease inhibitors (Sigma) were added to hippocampal tissue, and the samples were sonicated. Samples were centrifuged for 10 minutes at $14,000 \times g$ and 4°C , and the supernatants were pipetted out and placed in new tubes (Frank, Fonken, Annis, Watkins, & Maier, 2018). A Bradford assay was performed in order to analyze total protein concentration in each sample.

[...]

Enzyme-Linked Immunosorbent Assay (ELISA)

A rat IL-10 Quantikine ELISA kit (R&D Systems, Minneapolis, MN) was used to determine the protein levels of IL-10 in whole hippocampus tissue (García-Miguel et al., 2018). Absorbance data was used to determine levels of IL-10 protein in each sample. Data are not shown because the levels of IL-10 protein were too low to be detected.

[...]

Results

The purpose of this experiment was to determine whether colonization with *H. diminuta* altered the cytokine expression in the brain. Relative levels of mRNA expression were measured using qRT-PCR. Data were analyzed using the $2^{-\Delta\Delta\text{CT}}$ method. There were 8 animals in each group. Figure 19 shows mRNA expression of IL-10, IL-10 receptor, IL-13, TGF- β , IL-4 and IL-4 receptor. Levels of IL-10 mRNA were significantly increased ($P < 0.0001$), while levels of the IL-10 receptor were

significantly decreased ($P < 0.02$).

Upregulation of IL-10 expression contributes to an anti-inflammatory cytokine milieu, and the downregulation of IL-10R expression may be reflective of an increased release of IL-10. There was also a significant decrease in levels of IL-13 mRNA ($P < 0.0001$). Though IL-13 is typically an anti-inflammatory cytokine, it has also been linked to airway inflammation, which is characteristic in asthma, and *H. diminuta* have been known to decrease the risk of asthma. Levels of TGF- β , IL-4 and IL-4R mRNA showed no significant differences between helminth-colonized and control animals.

Discussion

These current results suggest that *H. diminuta* may not be an effective therapy for chronic pain; however, they are a promising treatment for neuroinflammation in the brain. [...]

In order to explore the molecular basis of helminth immunoregulation, qRT-PCR was performed to quantify the relative cytokine mRNA expression in the hippocampus (Figure 19). *H. diminuta* treatment upregulated mRNA expression of IL-10 and downregulated IL-10R, and both of these contribute to an

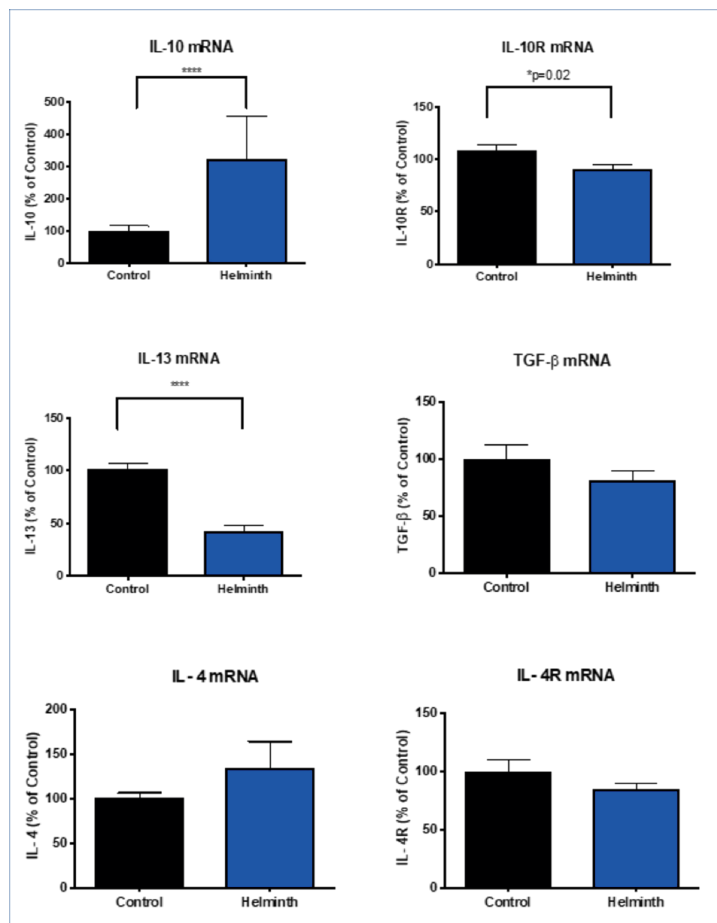


Figure 19: All qRT-PCR was performed on hippocampus tissue. IL-10 mRNA expression increased significantly in helminth-treated animals (**** $P < 0.0001$). IL-10R ($P = 0.02$) and IL-13 ($P < 0.0001$) mRNA decreased significantly in helminth-treated animals compared to control animals. There were no significant differences in IL-4, IL-4R, and TGF- β mRNA levels between groups (* $P < 0.05$, **** $P < 0.0001$). Real time PCR data were analyzed using the $2^{-\Delta\Delta CT}$ method.

anti-inflammatory cytokine milieu. Levels of IL-10 protein were undetectable in all samples of whole hippocampus tissue. IL-13 mRNA was downregulated, and this was expected, because IL-13 is responsible for airway inflammation and asthma (Corren, 2013). Though IL-13 can also play a role in anti-inflammatory processes, helminths are known to promote immunoregulation, which prevents the development of asthma and allergies (Parfrey et al., 2017; Graham A. W. Rook, 2012). TGF- β , IL-4, and IL-4R mRNA levels were not significantly impacted by *H. diminuta* treatment. IL-4 has been implicated in improved hippocampal-dependent memory (Chen et al., 2004, p. 4; Derecki et al., 2010). There was no consistent improvement in learning and memory behavior, and there was no significant upregulation of IL-4 or downregulation of its receptor in the hippocampus, so both behavioral results and molecular analysis support that *H. diminuta* colonization does not improve memory. [...]

The results from this project partially support the tenets of the hygiene hypothesis. Though behavioral results following CCI surgeries were inconclusive, molecular investigation of cytokine levels in the hippocampus showed promotion of an anti-inflammatory cytokine milieu due to the upregulation of IL-10 and downregulation of its receptor. These promising results guide future research toward investigation of cytokine levels in other brain regions, such as the amygdala. Additionally, the absence of consistent behavioral effects and presence of molecular changes in the brain suggest that the immunoregulation induced by *H. diminuta* may primarily influence the brain. This supports further research that investigates the effects

of helminth colonization on neuropsychiatric disorders. Finally, the potential unintended effects of *H. diminuta* colonization, such as increased carcinogenesis, must be examined in order to avoid the side effect of tumor growth and metastasis when establishing helminth immunotherapy. [...]

Works Cited

- Akkoc, T., Eifan, A. O., Ozdemir, C., Yazı, D., Yesil, O., Bahceciler, N. N., & Barlan, I. B. (2008). Mycobacterium vaccae Immunization to OVA Sensitized Pregnant BALB/c Mice Suppressed Placental and Postnatal IL-5 and Inducing IFN- γ Secretion. *Immunopharmacology and Immunotoxicology*, 30(1), 1–11. <https://doi.org/10.1080/08923970701812159>
- Bilbo, S. D., Wray, G. A., Perkins, S. E., & Parker, W. (2011). Reconstitution of the human biome as the most reasonable solution for epidemics of allergic and autoimmune diseases. *Medical Hypotheses*, 77(4), 494–504. <https://doi.org/10.1016/j.mehy.2011.06.019>
- Chen, L., Grabowski, K. A., Xin, J., Coleman, J., Huang, Z., Espiritu, B., ... Huang, H. (2004). IL-4 Induces Differentiation and Expansion of Th2 Cytokine-Producing Eosinophils. *The Journal of Immunology*, 172(4), 2059–2066. <https://doi.org/10.4049/jimmunol.172.4.2059>
- Chomczynski, P., & Sacchi, N. (1987). Single-step method of RNA isolation by acid guanidinium thiocyanate-phenol-chloroform extraction. *Analytical Biochemistry*, 162(1), 156–159. <https://doi.org/10.1006/abio.1987.9999>
- Corren, J. (2013). Role of interleukin-13 in

- asthma. *Current Allergy and Asthma Reports*, 13(5), 415–420. <https://doi.org/10.1007/s11882-013-0373-9>
- Cragg, J. J. (2018). Prevalence of chronic pain among individuals with neurological conditions. *Health Reports*, 29(82), 8.
- Dahlhamer, J. (2018). Prevalence of Chronic Pain and High-Impact Chronic Pain Among Adults — United States, 2016. *MMWR. Morbidity and Mortality Weekly Report*, 67. <https://doi.org/10.15585/mmwr.mm6736a2>
- Derecki, N. C., Cardani, A. N., Yang, C. H., Quinnes, K. M., Cribfield, A., Lynch, K. R., & Kipnis, J. (2010). Regulation of learning and memory by meningeal immunity: a key role for IL-4. *The Journal of Experimental Medicine*, 207(5), 1067–1080. <https://doi.org/10.1084/jem.20091419>
- Ege, M. J. (2017). The Hygiene Hypothesis in the Age of the Microbiome. *Annals of the American Thoracic Society*, 14(Supplement_5), S348–S353. <https://doi.org/10.1513/AnnalsATS.201702-139AW>
- Fairweather, D., & Cihakova, D. (2009). Alternatively activated macrophages in infection and autoimmunity. *Journal of Autoimmunity*, 33(3–4), 222–230. <https://doi.org/10.1016/j.jaut.2009.09.012>
- Frank, M. G., Fonken, L. K., Dolzani, S. D., Annis, J. L., Siebler, P. H., Schmidt, D., ... Lowry, C. A. (2018). Immunization with *Mycobacterium vaccae* induces an anti-inflammatory milieu in the CNS: Attenuation of stress-induced microglial priming, alarmins and anxiety-like behavior. *Brain, Behavior, and Immunity*, 73, 352–363. <https://doi.org/10.1016/j.bbi.2018.05.020>
- García-Miguel, M., Riquelme, J. A., Norambuena-Soto, I., Morales, P. E., Sanhueza-Olivares, F., Nuñez-Soto, C., ... Chiong, M. (2018). Autophagy mediates tumor necrosis factor- α -induced phenotype switching in vascular smooth muscle A7r5 cell line. *PLoS ONE*, 13(5). <https://doi.org/10.1371/journal.pone.0197210>
- Grange, J. M., Bottasso, O., Stanford, C. A., & Stanford, J. L. (2008). The use of mycobacterial adjuvant-based agents for immunotherapy of cancer. *Vaccine*, 26(39), 4984–4990. <https://doi.org/10.1016/j.vaccine.2008.06.092>
- Hernández-Pando, R., Aguilar, D., Orozco, H., Cortez, Y., Brunet, L. R., & Rook, G. A. (2008). Orally administered *Mycobacterium vaccae* modulates expression of immunoregulatory molecules in BALB/c mice with pulmonary tuberculosis. *Clinical and Vaccine Immunology: CVI*, 15(11), 1730–1736. <https://doi.org/10.1128/CVI.00286-08>
- Hewitson, J. P., Grainger, J. R., & Maizels, R. M. (2009). Helminth immunoregulation: The role of parasite secreted proteins in modulating host immunity. *Molecular and Biochemical Parasitology*, 167(1–9), 1–11. <https://doi.org/10.1016/j.molbiopara.2009.04.008>
- Liu, A. H. (2015). Revisiting the hygiene hypothesis for allergy and asthma. *Journal of Allergy and Clinical Immunology*, 136(4), 860–865. <https://doi.org/10.1016/j.jaci.2015.08.012>
- McKenney, E. A., Williamson, L., Yoder, A. D., Rawls, J. F., Bilbo, S. D., & Parker, W. (2015). Alteration of the rat cecal microbiome during colonization with the helminth *Hymenolepis diminuta*. *Gut Microbes*, 6(3), 182–193. <https://doi.org/10.1080/19490976.2015.1047128>
- Parfrey, L. W., Jirků, M., Šíma, R., Jalovecká,

- M., Sak, B., Grigore, K., & Pomajbíková, K. J. (2017). A benign helminth alters the host immune system and the gut microbiota in a rat model system. <https://doi.org/10.1371/journal.pone.0182205>
- Rook, Graham A. W. (2012). Hygiene Hypothesis and Autoimmune Diseases. *Clinical Reviews in Allergy & Immunology*, 42(1), 5–15. <https://doi.org/10.1007/s12016-011-8285-8>
- Smyth, K., Morton, C., Mathew, A., Karuturi, S., Haley, C., Zhang, M., ... Parker, W. (2017). Production and Use of *Hymenolepis diminuta* Cysticercoids as Anti-Inflammatory Therapeutics. *Journal of Clinical Medicine*, 6(10), 98. <https://doi.org/10.3390/jcm6100098>
- Stanford, J., Stanford, C., & Grange, J. (2004). Immunotherapy with *Mycobacterium vaccae* in the treatment of tuberculosis. *Frontiers in Bioscience: A Journal and Virtual Library*, 9, 1701–1719.
- Villeneuve, C., Kou, H. H., Eckermann, H., Palkar, A., Anderson, L. G., McKenney, E. A., ... Parker, W. (2018). Evolution of the hygiene hypothesis into biota alteration theory: what are the paradigms and where are the clinical applications? *Microbes and Infection*, 20(3), 147–155. <https://doi.org/10.1016/j.micinf.2017.11.001>
- Williamson, L. L., McKenney, E. A., Holzknicht, Z. E., Belliveau, C., Rawls, J. F., Poulton, S., ... Bilbo, S. D. (2016). Got worms? Perinatal exposure to helminths prevents persistent immune sensitization and cognitive dysfunction induced by early-life infection. *Brain, Behavior, and Immunity*, 51, 14–28. <https://doi.org/10.1016/j.bbi.2015.07.006>
- Zhang, M., Mathew, A. J., & Parker, W. (2018). Production of *Hymenolepis diminuta* in the Laboratory: An Old Research Tool with New Clinical Applications. *Methods in Molecular Biology (Clifton, N.J.)*, 1799, 27–38. https://doi.org/10.1007/978-1-4939-7896-0_3

Examining the Glacial Mass Balance of the Arikaree Glacier, Front Range, Colorado Using GIS and Degree Day Methods

Kevin Knopp

The following is an excerpt from a longer piece. For full text, please visit <https://www.colorado.edu/honorsjournal/sites/default/files/attached-files/examiningtheglacialmassbalance.pdf>

ABSTRACT

The health of glaciers around the world is threatened by anthropogenic climate change as rising temperatures and changing precipitation patterns affect mass balance of glaciers. The manifestations of global climate vary at the regional level, in both magnitude and direction of temperature and precipitation changes. For this reason, glacier response is not expected to be uniform across different seasons and in different places. Based on precipitation totals and wind patterns, there is evidence that alpine glacier mass balance might actually be positive in some locations. This study focuses on the Arikaree Glacier in the Front Range of Colorado, USA. I use snow depth measurements taken on the glacier at peak accumulation and measured air temperatures to derive a degree day calculation of ablation and to produce a plausible mass-balance for each year from 1997 to 2017. I found that the Arikaree Glacier has experienced a negative mass balance each year since 1997. Future research should utilize a more detailed approach to this form of mass balance calculation and assess other small mid-latitude glaciers to see if they are experiencing the same results.

INTRODUCTION

Mass balance studies of glaciers are

good indicators of climate change, particularly small cirque glaciers (Barreto, 1994). This is because there is no distinct accumulation and ablation areas, so the entire glacial surface is more responsive to changes in surface mass balance. Increasing temperatures from anthropogenic climate change are causing many glaciers to melt and experience negative mass balance (Gregory, Stocker, Lemke, & Bindoff, 2007). This is particularly noticeable in higher latitude, maritime environments where small changes in temperatures are causing lower elevation snow to melt out or even fall as rain in the winter season. [...]

The Indian Peaks receive roughly 35-60 inches (~89-152 cm) of precipitation each year, well above the average of 15.47 inches (~39 cm) for the state of Colorado (National-Atlas, 2005). Winter weather is generally cold and windy, with some gusts reaching above 20 m/s in velocity (Barreto, 1994). Summers are typically mild and much less windy than winters. Temperatures can get above 60 °F (~15.5 °C) on the high peaks and afternoon thunderstorms are notorious (Barreto, 1994). Inconsistencies in weather also occur during summer. Some summers can be wet and stormy, and others hot and dry. These climate factors heavily influence the mass balance of the Arikaree Glacier (Barreto, 1994; Johnson,

1979).

Two major mass balance studies have already been done on the Arikaree Glacier. The first was done by James Johnson in 1979 and the other was done by Henrique Barreto in 1994. These mass balance studies involved stake methods to measure the ablation and were conducted using data collected over multiple years: 1969-1974 (Johnson, 1979) and 1992-1993 (Barreto, 1994). Both revealed that the overall swings of positive or negative mass balance are largely influenced by how stormy the ablation (summer melt) season is. If the ablation season is stormy, there is increased cloud cover, which inhibits the amount of incoming direct solar radiation on the glacier (Johnson, 1979). Due to the high variability in net mass balance of the Arikaree Glacier, some years can yield large positive mass balances and others can be large negative mass balances.

[...]

Despite increasing temperatures globally, there is reason to believe that the Arikaree Glacier might actually be gaining size due to recent findings that indicate greater precipitation totals in winter and small increasing trends in precipitation during summer (Kittel et al., 2015). The increasing trends in precipitation are observed at nearby climate station D-1 (Fig. 2), which show large increases in winter precipitation over a long period indicating that more snowfall is occurring on average. There is also a slight increase in precipitation during summer, giving reason to believe that summers are stormier as well. Stormier summers would indicate more cloud cover to limit the ablation on the glacier. Kittel et al. (2015) conclude that the D-1 site experienced significant increasing trends in winter precipitation due

to changes in synoptic weather patterns across North America and changes in precipitation generation from mesoscale interaction of synoptic circulation with local topography. They found increases of 21-126% monthly winter time precipitation totals at the D-1 site. It was concluded that a shift from southwesterly to northwesterly winds favored more orographic uplift and increased precipitation on the windward side of the Continental Divide, as well as the areas just east of the divide due to a "spillover" effect. Southwesterly winds favor precipitation in the lower elevations and northwesterly winds favor precipitation in high elevations (Kittel et al., 2015).

[...]

By obtaining accumulation and ablation data, a mass balance can be calculated over twenty-one years. The health of the Arikaree Glacier can then be determined and give insight into the fate of other glaciers in Colorado's Front Range and potentially see if there are other small mid-latitude alpine glaciers around the world experiencing the same results as the Arikaree Glacier. It might also provide further research opportunities to study how areas are experiencing increased levels of precipitation and gains in snow accumulation.

BACKGROUND

The Arikaree Glacier is nestled in between Arikaree Peak and Navajo Peak in Colorado's Front Range Indian Peak Wilderness Area (Fig. 2). The location coordinates of the Arikaree Glacier are 40°3'10"N 105°38'20"W (Johnson, 1979). The majority of the glacier sits at the base of Arikaree Peak but extends out toward Navajo Peak in a half moon shape. The glacier is

located within the Green Lakes Valley as part of the upper Boulder Creek watershed. The northern boundary of the watershed is Niwot Ridge, where alpine research occurs as part of the Niwot Ridge Long-Term Environmental Research (LTER) program within the University of Colorado's Mountain Research Station. [...]



Figure 2. Oblique aerial Google Earth image of the Arikaree Glacier and surrounding Green Lakes Valley. The Arikaree Glacier sits at the head of the Green Lakes Valley beneath the north side of Arikaree Peak. Image is viewed looking southwest. Green line indicates Continental Divide.

METHODS

Temperature and Precipitation

Data collection in order to determine the mass balance of the glacier involved field measurements on the glacier as well as data from the Niwot Ridge LTER website. This data is part of the LTER program through the Institute for Arctic and Alpine Research (INSTAAR) and the University of Colorado. Temperature data for the D-1 site on Niwot Ridge was used to evaluate temperature trends (Losleben, 2006a). This data was used to assess temperature changes on Niwot Ridge since the completion of Barreto's study

in 1993. Air temperature at the D-1 site was analyzed from November 1, 1993 to present. The data used in this study was selected to start on November 1, 1993 in order to correspond with the start of the next glacial accumulation-ablation season following the completion of the study of Barreto (1994). [...]

For recent precipitation trends, precipitation data was collected at the D-1 site and sorted to obtain days that recorded a value for precipitation. In other words, the dates with 'no data' or a '0' were filtered out. Next, the data was broken up into winter months (October-May), assuming that all of this precipitation fell as snow and contributed to accumulation on the glacier. The values were summed for each winter to give a precipitation total for that season. [...]

Accumulation

For accumulation data on the Arikaree Glacier, a snow pit was dug on the east side of the glacier near the moraine and glacial pool. The total snow depth as well as snow density were measured in order to calculate the snow water equivalent. As part of the annual Snow Survey, conducted at peak SWE, around 500 other point samples (some on the glacier) were recorded throughout Green Lakes Valley to help with estimating the depth of snow on the glacier for the winter year accumulation. For each year, the snow depth measurements and coordinates were put into the ArcGIS program. I ran the Inverse Distance Weighting tool to help estimate the different snow accumulation totals on different parts of the glacier. [...]

Ablation

A degree day method was used to estimate summer ablation for each season based on the average air temperature values. Temperature index degree day methods are a very common way of measuring ablation due to the wide availability of air temperature data, relatively easy interpolation and forecasting possibilities of air temperature, generally good model performance despite simplicity, and the simplicity of computation (Hock, 2003). Temperature index degree day methods have a high correlation with air temperature because both sensible and latent heat fluxes are heavily affected by air temperature. [...]

Days above 0 °C are assumed to have melting occurring. The positive air temperature days were then summed up for each ablation season and then multiplied by a degree day factor. The degree day factor is a coefficient that the days above 0 °C sum is multiplied by and is based on a range of factors including latitude, humidity, maritime or continental climate, etc. [...]

Mass Balance

Once there were accumulation and ablation estimates for the glacier, the annual mass balance was calculated by subtracting the total ablation from the total accumulation (accumulation - ablation). If this value was positive, then the glacier gained mass for the year. If the value was negative, then the glacier lost mass for the year. By doing this over the course of the study (years 1997-2017), one of three different scenarios could be concluded: either the glacier is gaining size overall, losing size overall, or the mass balance varies from year to year and there is no overall trend in the data. [...]

RESULTS

Over the study period, a linear regression shows a -0.0002 °C/day slope in the air temperature at the D-1 site, suggesting that the average air temperature is actually getting colder in the alpine environment on Niwot Ridge. Precipitation data revealed that there is an increase in winter precipitation at site D-1 by an amount of 1.94 mm per year. [...]

Accumulation estimates on the Arikaree Glacier vary significantly from year to year. The average snow accumulation for a given year was about 3.90 meters. A statistical t-test revealed that there is a significant trend in the negative direction of snow water equivalent accumulation. Total ablation for years 1997-2017 yielded an average of 3.9 meters of water equivalent (w.e.) being melted each year. After conducting a t-test for snow water equivalent ablation, I found that there is also a significant negative trend. Each year of the study yielded a negative mass balance. However, the negative value for net balance varied considerably from year to year (Figure 7). Some years were very close to reaching equilibrium while other years were largely negative. The largest negative year occurred in 2007 with over 5 meters of water equivalent loss and the smallest negative year occurred in 2014 with a 0.3-meter loss in water equivalent. A t-test showed that the positive trend in net balance is significant. [...]

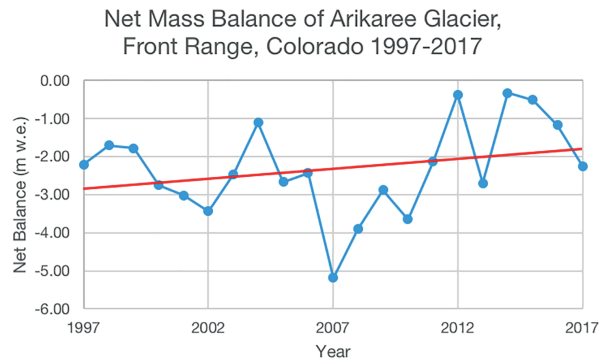


Figure 7. Graph showing net mass balance for the Arikaree Glacier from 1997-2017. There has been a negative net mass balance each year; however, in recent years, the net mass balance has been nearing equilibrium. Most notable is the large negative year in 2007 which had over 5 meters of water equivalent loss.
[...]

DISCUSSION

Despite an increase in global mean temperatures, the Arikaree Glacier is actually getting colder. Believed to be due to shifts in wind patterns, this change is also leading to increased precipitation levels (Kittel et al., 2015). Both of these factors provide evidence for favorable conditions for glacier growth or positive mass balances.
[...]

It can be concluded that the mass balance of each year is heavily determined by the ablation season. The winter year of 2016-2017 was considered to be a large snow year for Colorado statewide, yet the mass balance was still negative due to a large ablation season. The same pattern can be seen in the year 2009.
[...]

Despite the overall positive trend in the net mass balance toward equilibrium, the

overall health of the Arikaree Glacier is poor since every year of the study produced a negative net mass balance. The temperature and precipitation conditions are favorable for a positive net mass balance, but heavy ablation during the summer months are prohibiting this, especially when certain years contain large ablation factors, such as the one seen in 2007. This could be attributed to decreased cloud cover in summer months allowing for more direct incoming sunlight to hit the glacier and/or impurities such as dust and soot deposition lowering the albedo of the surface and resulting in faster melting.
[...]

CONCLUSION

The overall health of glaciers around the world are being threatened by climate change. However, due to micro-climate variability and changes in precipitation and wind patterns, there is evidence to believe that some glaciers may be experiencing positive mass balances. My study calculated the net mass balance for the Arikaree Glacier, Front Range, Colorado, USA to assess the overall health of the glacier over the course of 21 years. Over the course of 21 years, the Arikaree Glacier has had a negative mass balance each year, but the negative value varies considerably from year to year. These results provide incentive for further research of the Arikaree Glacier in order to achieve a more detailed and accurate study of the mass balance as well as further research of other high alpine, mid-latitude glaciers in order to see if they are experiencing similar results as the Arikaree Glacier.

WORKS CITED

- Barreto, H. (1994). *An Investigation of the 1991-1993 Mass Balance Arikaree Glacier, Front Range, Colorado*. University of Colorado-Boulder.
- Gregory, J., Stocker, T., Lemke, P., & Bindoff, N. (2007). *Climate Change 2007: The Physical Science Basis*.
- Hock, R. (2003). Temperature index melt modelling in mountain areas. *Journal of Hydrology*. [https://doi.org/10.1016/S0022-1694\(03\)00257-9](https://doi.org/10.1016/S0022-1694(03)00257-9)
- Johnson, J. (1979). *Mass Balance and Aspects of the Glacier Environment, Front Range, Colorado, 1969-1973*. University of Colorado-Boulder.
- Kittel, T. G. F., Williams, M. W., Chowanski, K., Hartman, M., Ackerman, T., Losleben, M., & Blanken, P. D. (2015). Contrasting long-term alpine and subalpine precipitation trends in a mid-latitude North American mountain system, Colorado Front Range, USA. *Plant Ecology and Diversity*, 8(5-6), 607-624. <https://doi.org/10.1080/17550874.2016.1143536>
- Losleben, M. (2006a). Air Temperature data for D1 chart recorder, 1952-ongoing. Retrieved from <https://doi.org/10.6073/pasta/c241a710028b578ac62ddec47eb0d5e9>.
- Losleben, M. (2006b). Precipitation data for D1 chart recorder, 1964-ongoing. Retrieved from <https://doi.org/10.6073/pasta/6aebd32af0f8c8af69dd3c89f9e602a6>.
- National-Atlas. (2005). *Precipitation-Colorado*. Retrieved from https://nationalmap.gov/small_scale/printable/images/pdf/precip/pageprecip_co3.pdf

Accounting for Confinement Shifts on the Binding Energies of ^{39}K Feshbach Molecules

Jared Popowski

The following is an excerpt from a longer piece. For full text, please visit https://scholar.colorado.edu/concern/undergraduate_honors_theses/5m60qs924

Summary

Ultracold atomic gases have many fascinating and unintuitive properties, as their extremely low temperatures bring out their inherent quantum nature. One such property is the phenomenon of a *Feshbach resonance*, in which an applied magnetic field of a particular strength allows for fully tunable interactions between particles in the gas. Near a Feshbach resonance, one can form two-particle bound states called *Feshbach molecules*, and measurements of these molecules' properties such as their binding energies can tell us important information about the behavior of the gas. We consider here a correction to our recent ^{39}K Feshbach molecule binding energy data, which takes into account the magnetic trap used to hold our gas up against gravity in our experimental system. The presence of this trap shifts the binding energies that we measure in the lab slightly away from their "true" free-space values, and calculating this so-called confinement shift requires an understanding of two-particle quantum mechanical scattering theory. After briefly reviewing the relevant physics, as well as our experimental setup and procedure for producing Feshbach molecules, we develop a MATLAB program to numerically simulate the confinement shift for different atomic

species and magnetic trap configurations.

The program is first used to replicate the confinement shift for ^6Li Feshbach molecules calculated recently by another group, before finally applying it to correct our own measurements of ^{39}K Feshbach molecules. The correction of these measurements is necessary for our determination of the Feshbach resonance location with unprecedented accuracy.

Abstract

Ultracold ^{39}K gases provide an ideal platform to study quantum few- and many-body systems, due to the high degree of control present in these systems. In particular, Feshbach resonances facilitate a magnetically tunable interaction strength between the atoms in the gas, and allow the formation of two- and three-body bound states, called Feshbach molecules and Efimov trimers respectively. Radio-frequency dissociation spectroscopy of weakly bound Feshbach molecules is one of the most precise ways to characterize the properties of a Feshbach resonance. We apply a numerical method to our Feshbach molecule binding energy data to compute the shift in the molecule's binding energy due to the presence of a confining potential. These simulations are first used to replicate the confinement

shift found for ${}^6\text{Li}$ Feshbach molecules by another group, and then to correct our measurement results for the binding energy of ${}^{39}\text{K}$ Feshbach molecules. The correction of these measurements is necessary for our determination of the Feshbach resonance location with unprecedented accuracy. [...]

Chapter 2

Two-Particle Scattering and the Theory of Feshbach Resonances

2.2 Basic Physics of Feshbach Resonances and Feshbach Molecules

Imagine an atom with two molecular potentials, V_{bg} and V_c , which represent two different scattering processes between a pair of the atoms (see Figure 2.2). The molecular potential $V_{bg}(R)$ (where $r = R$ is the radial separation of the atoms) is the potential that two free atoms encounter when coming in from $R \rightarrow \infty$, and it is hence the energetically open channel for a collision process having the near-zero energy $E \rightarrow 0$. This is why we call V_{bg} the *open channel*, or alternatively the *entrance channel*. The other potential $V_c(R)$ can support a molecular bound state (in Figure 2.2, this bound state has an energy E_c) near the threshold of the open channel.

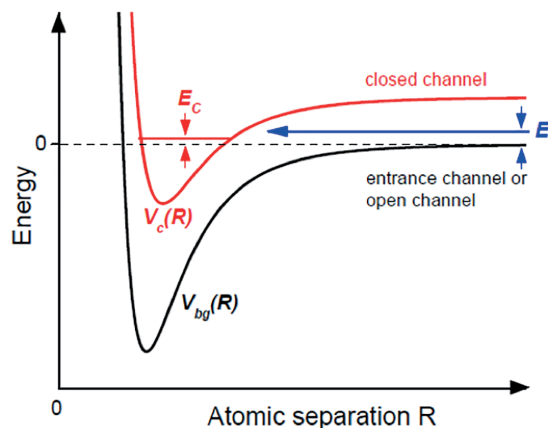


Figure 2.2: A simple two-channel model of a Feshbach resonance. Image obtained from [8].

A *Feshbach resonance* occurs when this bound state energetically approaches the asymptotic potential energy $E = 0$ in the open channel, modifying the scattering in the open channel.

Hence it is clear that in order to have a Feshbach resonance, we need some way to control the energy difference between the molecular bound state and the collision energy in the open channel. In most cases (including our specific case with ${}^{39}\text{K}$), this is obtained by ensuring that the potentials V_{bg} and V_c have different magnetic moments: this allows the energy difference between the two channels to be controlled via a magnetic field. Feshbach resonances in these cases are referred to as *magnetically tuned Feshbach resonances*. If B is varied so that it passes through a Feshbach resonance, the scattering length a changes dramatically, increasing or decreasing to $\pm\infty$, jumping discontinuously to $\mp\infty$, and then returning to a value close to its original off-resonant value [4]. One can describe a magnetically tuned Feshbach resonance by a simple equation for the s-wave scattering-length a as a function of the applied magnetic field B [20],

$$a(B) = a_{bg} \left(1 - \frac{\Delta}{B - B_0} \right), \quad (2.9)$$

where a_{bg} is the *background scattering length*, denotes the *resonance position* where the scattering length diverges ($a \rightarrow \pm\infty$), and Δ is the *resonance width*, measured in units of the magnetic field.

Equation (2.9) is plotted as a function of B in panel (a) of Figure 2.3.

The coupling of the bound state to the open channel threshold creates a coupled state with energy E . On the $a < 0$ side of the Feshbach resonance, E is positive and the coupled

state is “virtual,” meaning that it influences the scattering but is not an accessible state. For $a > 0$, the coupled state is a real molecular state, because E is below the continuum. We call such a molecular state a Feshbach molecule, or a Feshbach dimer. The binding energy of a Feshbach molecule for large positive values of a is approximated by

$$E_b = \frac{\hbar^2}{2\mu a^2} = \frac{\hbar^2}{ma^2}. \quad (2.10)$$

Therefore, in the limit of large positive a , E_b depends quadratically on the detuning $B - B_0$. This results in the bend seen in the inset to panel (b) of Figure 2.3, where we have plotted the dressed state energy E as a function of B near a magnetically tuned Feshbach resonance.

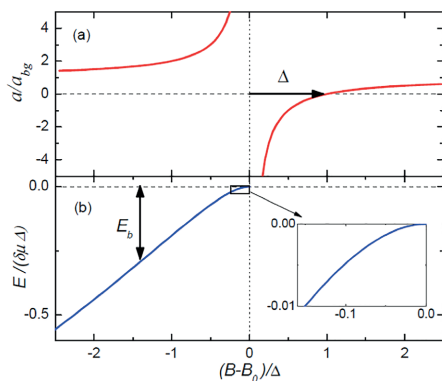


Figure 2.3: A plot (a) of the s-wave scattering length a and (b) of the dressed state energy E near a magnetically tuned Feshbach resonance. The binding energy is defined to be positive, $E_b = -E$. The inset shows the universal regime near the resonance position where a is very large and positive. Image obtained from [8].
[...]

Chapter 3 Apparatus and Measurement of Feshbach Molecules

3.3 Production and Measurement of Feshbach Molecules

We use magneto-association [14,23] to create a macroscopic population of Feshbach molecules for our binding energy measurements. This technique has historically resulted in the largest molecular populations; in 2005, a JILA lab measured atom-dimer conversion efficiencies of around 50% for the magneto-association of a ^{85}Rb Bose gas system [15]. However, our current setup is more challenging, and a significant amount of our ^{39}K atoms ($> 80\%$) remain unpaired after the sweep. Since we need 10^3 - 10^4 Feshbach molecules for an adequate signal for RF spectroscopy, the atomic samples required before the sweep are on the order of $\sim 10^5$ atoms.

Magneto-association is generally accomplished with a time-varying magnetic field near a Feshbach resonance. A slow adiabatic sweep of the magnetic field through the resonance into the region where bound molecules exist causes the association of atoms into very weakly bound Feshbach molecules [14,15]. This makes intuitive sense when we consider that the bound molecular state becomes degenerate with the free atom continuum at the location of the Feshbach resonance. In our experiment, we begin by producing a thermal sample of atoms far from the resonance on the $a > 0$ side, before rapidly ramping to the $a < 0$ side of the resonance (dashed red arrow on the top in Fig. 3.5). We then form our molecules by slowly sweeping the magnetic field back to the positive side of the resonance, depicted in Fig. 3.5 by the dashed red arrow on the bottom. Finally, we

apply a sequence of cleaning pulses to blast away unconverted atoms, leaving behind a pure molecular gas.

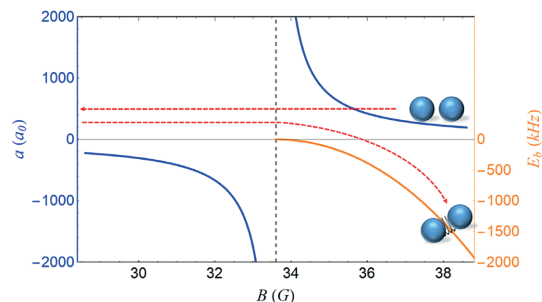


Figure 3.5: A diagram of magneto-association of Feshbach molecules near the $B_0 = 34$ G resonance in the ^{39}K hyperfine state $|F = 1, m_F = -1\rangle$. Two unpaired atoms are adiabatically transferred to the molecular state with magnetic field ramps, which are depicted by the dashed red arrows. Image obtained from [6].

After a pure molecular gas is produced, the magnetic field is ramped to various values, corresponding to different binding energies, where we perform RF dissociation spectroscopy. From these measured binding energies, we can very precisely determine the position and the width of our Feshbach resonance of interest [8].

[...]

Due to the stability of our magnetic field and high degree of control over other experimental sources of error, our binding energy data has unprecedented precision, and an accurate determination of the Feshbach resonance location requires consideration of additional sources of error. The biggest systematic error affecting our molecular spectra arises from the confining potential, used to hold the atoms up against gravity. To accurately determine the

binding energy of the molecules, we have to subtract the effects of the confining potential from the dissociation frequency $\delta\nu$ [30]. The shift on our measured binding energies due to the confining potential is referred to as the *confinement shift*. Both the initial and final states for the RF dissociation have confinement shifts associated with them, and the total confinement shift is the difference between the final state shift and the initial state shift.

[...]

Chapter 4

Confinement Shift for Feshbach Molecules in a Trap

4.1 Intuition

We can understand the confinement shift intuitively by building up a qualitative picture of the effects of confinement on Feshbach molecules. We introduce the relevant physics step-by-step in Figure 4.1.

Part a of the figure depicts the continuum of scattering states available to two free atoms, since they are allowed to have any nonnegative value for the relative motional energy $E = \hbar^2 k^2 / (2\mu)$. In free space, where a confining potential is not required to keep the atoms in place, dissociation of a Feshbach molecule with binding energy E_b would involve dissociation into these free atom continuum states. This is represented in part b of Figure 4.1, where we use a van der Waals tail $U(\mathbf{r}) = -C_6/r^6$ to represent the molecular potential (ignoring the short-range $1/r^{12}$ repulsive part of the potential for visual simplicity). However, on Earth we need a way to prevent the atoms from falling out of our system under the influence of gravity, and so we introduce a confining potential to hold up the atoms. In part c of Figure 4.1, we show the potential energy and first three energy levels

for a harmonic trap $V_t(\mathbf{r}) = \frac{1}{2}m\omega^2r^2$. Once the trap is introduced, the continuum of free atom scattering states that was previously present becomes the discrete energy levels of the trap. However, we note that in practice the experimental resolution may be insufficient to resolve the trap levels, in which cases the final state of dissociation can be well-described by a continuum [30]. Adding together the effects of the molecular potential and the confining potential, we end up with the potential curve depicted in part d of Figure 4.1. In the figure, the dashed navy blue curve gives the original form of the confining potential, and the dashed light blue curve gives the original form of the molecular potential. The binding energy of a Feshbach molecule with free-space binding energy E_B is perturbed to the new value E_{B_t} by the harmonic trap, and similarly the energy levels in the trap that the dissociated atoms occupy are perturbed by the molecular potential.

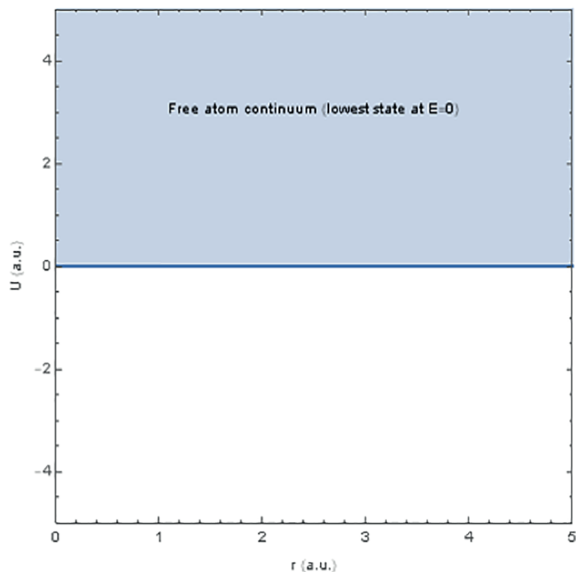


Figure 4.1a: The scattering state for two free atoms can have any nonnegative value for the relative motional energy $E = \hbar^2 k^2 / (2\mu)$, with the minimum-energy scattering state

occurring for $E = 0$. This means that for two atoms in free space, there is a continuum of scattering states, represented in the plot by a shaded region for $U > 0$. Here r is the interparticle separation.

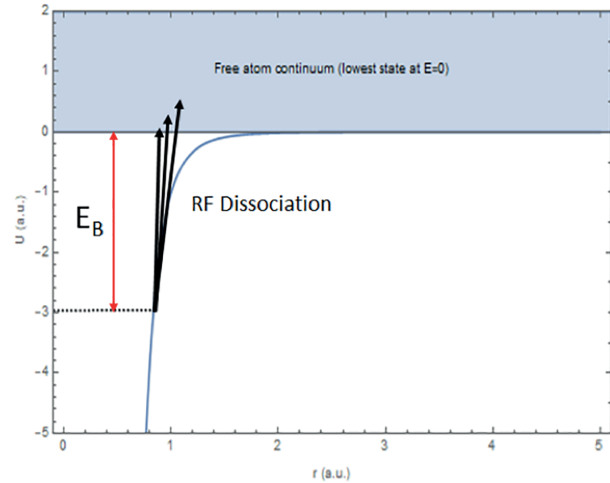


Figure 4.1b: The dissociation of a Feshbach molecule with binding energy E_B in free space, where the blue curve is a van der Waals tail $U(r) = -C_6/r^6$ representing the molecular potential and the final states are the free atom continuum states from the previous part of the figure (r is the interparticle separation). The black arrows illustrate the fact that the molecule does not necessarily have to dissociate into the $E = 0$ state, since there is some probability of dissociating into a higher energy continuum state for a higher frequency RF pulse. This is evidenced by the long tails on our measured dissociation spectra in Figure 3.7.

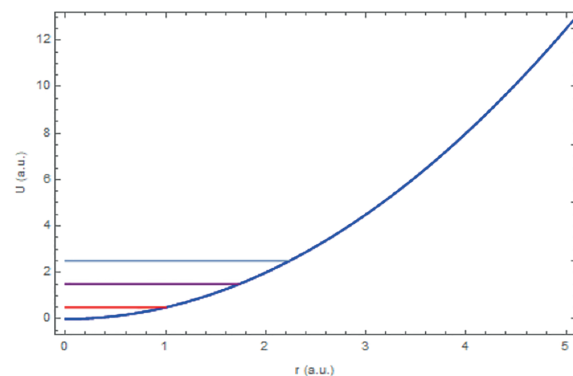


Figure 4.1c: The introduction of a confining potential (here a harmonic potential $V_t(\mathbf{r}) = \frac{1}{2}m\omega^2\mathbf{r}^2$) takes the continuous energy spectrum of the scattering states for two free atoms and restricts it to the discrete energy levels of the trap, the first three of which are given in the plot.

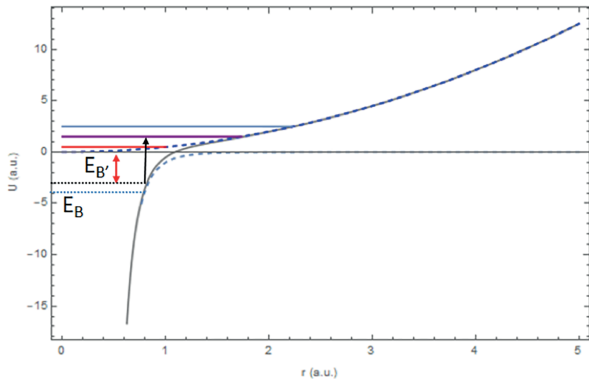


Figure 4.1d: The full story of Feshbach molecule dissociation into a trap, where the molecular potential in part b and the confining potential in part c have been added together. The dashed navy blue curve gives the unperturbed form of the confining potential, and the dashed light blue curve below gives the unperturbed form of the molecular potential. The confining potential perturbs the binding energy of a Feshbach molecule from its free space value E_B to the new value $E_{B'}$ (the difference on this plot is exaggerated for clarity), and the molecular potential perturbs the discrete trap states for the final dissociated free atoms. [...]

4.3 Theory of the Confinement Shift for Two Atoms in a Harmonic Trap

While Equation (4.1) for the final state shift and our perturbation theory approach for the initial state shift provide good intuition for the confinement shift, they are only approximations, and do not describe the

true energy spectrum of an interacting two-body quantum system in a trap. To obtain the accurate confinement shift on our measurements of ^{39}K Feshbach molecules, we require some more theory.

[...]

Following this procedure, a 2006 PRA paper by Zbigniew Idziaszek and Tommaso Calarco [17] found the following expression determining the energy levels for $m = 0$,

$$-\frac{\sqrt{\pi}}{a} = \mathcal{F}(-\mathcal{E}/2), \quad (4.8)$$

where

$$\mathcal{F}(x) = \int_0^\infty dt \left(\frac{\eta e^{-xt}}{\sqrt{1 - e^{-t}}(1 - e^{-\eta t})} - \frac{1}{t^{3/2}} \right), \text{ for } x > 0. \quad (4.9)$$

Here $\eta = \omega_\perp/\omega_z$ is the aspect ratio of the system and $\mathcal{E} = E - E_0$ denotes the energy shifted by the zero-point oscillation energy $E_0 = 1/2 + \eta$. This is the main result that we were interested in, as this gives us the shifted energy levels due to confinement in an axially symmetric harmonic trap. The validity of the integral representation (4.9) is limited to $\mathcal{E} < 0$, which is sufficient for our purposes, but this result can be extended to energies $E > E_0$ through analytic continuation [17].

Chapter 5 Testing and Results of My Confinement Shift Program

To calculate the confinement shift to the measured binding energies of our Feshbach molecules, I wrote a MATLAB program that numerically solves Equations (4.8) and (4.9). In the following sections, I describe how the program works, what I did to test the program, and the final results for the confinement shifts

to our measured ^{39}K binding energies.

[...]

We are not the first experiment to reach the level of precision where the effect of the confinement shift must be accounted for: a 2013 work detailed in reference [30] used the method of RF dissociation to measure a Feshbach resonance location in ^6Li with unprecedented precision, and included the effects of the confining potential by solving Equations (4.8) and (4.9) for their system, just as we aim to do. Hence a good test for my MATLAB program is whether it reproduces the results that the authors of reference [30] obtained for the confinement shift, when I give the program all of the necessary trap parameters ($\eta = 10$) and constants for ^6Li .

[...]

In short, my program successfully reproduced the confinement shifts found in [30] for all values of the measured binding energies, with discrepancies much smaller than the experimental errors on the measurements.

[...]

5.3 Results for the Confinement Shift to our ^{39}K Feshbach Molecules

After verifying that my program was able to reproduce the confinement shifts found for the ^6Li binding energy data, we needed to do the same procedure to find the confinement shifts for our own ^{39}K binding energy data.

Our trap is axially symmetric with a radial trap frequency $\omega_r/2\pi = 28.64(66)$ Hz in the (x, y) -plane and an axial trap frequency of $\omega_z/2\pi = 117.3(1.0)$ Hz, so the trap aspect ratio is $\eta = \omega_r/\omega_z \approx 0.244$. Using this value and the relevant constants for ^{39}K , we obtained the free space and confined binding energy curves displayed in Figure 5.3.

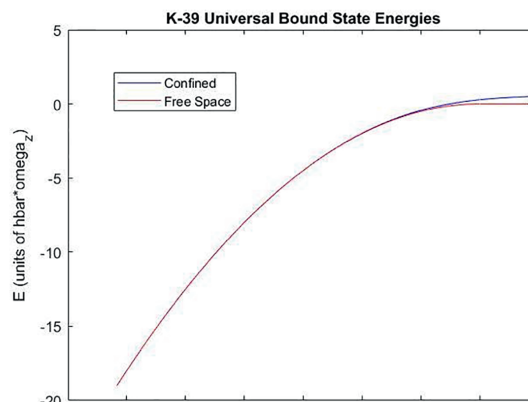


Figure 5.3: The computed free space and confined ^{39}K Feshbach molecule binding energies. The energy units are $\hbar\omega_z = 2\pi\hbar\nu_z$ and the length units are the oscillator length $a_z = \sqrt{(\hbar/\mu\omega_z)}$.

For the final state $|F = 2, m_F = 0\rangle$ after dimer dissociation, the associated scattering length is very small compared to the harmonic oscillator length (corresponding to very far out to the right in Figure 5.3), so the confinement-related energy shift of our final state is essentially equal to the zero-point energy of our trap, $E_0/h = 87.3$ Hz.

Therefore, the total confinement-related shift is similar for all of our measurements and is approximately equal to the zero-point energy $E_0/h = 87.3$ Hz, to within 1.4 Hz uncertainty on our trapping frequencies. We subtract the total confinement shift from the measured dissociation threshold frequency to extract the dimer binding energy E_b/h in free space; see Figure 5.6 for our final binding energy results.

[...]

Chapter 6 Conclusion and Future Directions

[...]

There are still many open questions left to explore in the realm of few-body and universal physics with ultracold Bose gases.

In particular, this thesis focused only on our work characterizing the two-body physics that arises from Feshbach resonances, but there is a rich spectrum of three-body and four-body physics tied to Feshbach resonances which has yet to be fully and precisely characterized. Common problems with previous work in this area include failing to account for systematic effects such as finite temperature effects, incorrect density calibrations, and so on. Just as we have accounted for the confinement shift in this work, our lab aims to account for these systematic effects to obtain precision data that can serve as a benchmark for comparisons with theories. Such careful measurements are vital towards the goal of building a “ground up” understanding of quantum many-body physics through precise characterizations of quantum few-body physics.

Works Cited

- [1] MA Baranov, Klaus Osterloh, and M Lewenstein. Fractional quantum hall states in ultracold rapidly rotating dipolar fermi gases. Physical review letters, 94(7):070404, 2005.
- [2] Hans Bethe and Rudolf Peierls. Quantum theory of the dipton. Proceedings of the Royal Society of London. Series A-Mathematical and Physical Sciences, 148(863):146–156, 1935.
- [3] Immanuel Bloch. Quantum coherence and entanglement with ultracold atoms in optical lattices. Nature, 453(7198):1016, 2008.
- [4] Eric Braaten and H-W Hammer. Universality in few-body systems with large scattering length. Physics Reports, 428(5-6):259–390, 2006.
- [5] Thomas Busch, Berthold-Georg Englert, Kazimierz Rzazewski, and Martin Wilkens. Two cold atoms in a harmonic trap. Foundations of Physics, 28(4):549–559, 1998.
- [6] Roman Chapurin. Precise Measurements of Few-Body Physics in Ultracold 39k Bose Gas. PhD thesis, University of Colorado Boulder, 2019. Physics Graduate Theses & Dissertations. 289. https://scholar.colorado.edu/phys_gradetds/289.
- [7] Roman Chapurin, Xin Xie, Michael J Van de Graaff, Jared S Popowski, Jose P D’Incao, Paul S Julienne, Jun Ye, and Eric A Cornell. A precision test of the limits to universality in few-body physics. arXiv preprint arXiv:1907.00729, 2019.
- [8] Cheng Chin, Rudolf Grimm, Paul Julienne, and Eite Tiesinga. Feshbach resonances in ultracold gases. Reviews of Modern Physics, 82(2):1225, 2010.
- [9] Cheng Chin and Paul S Julienne. Radio-frequency transitions on weakly bound ultracold molecules. Physical Review A, 71(1):012713, 2005.
- [10] Jean Dalibard, Fabrice Gerbier, Gediminas Juzeliūnas, and Patrik Öhberg. Colloquium: Artificial gauge potentials for neutral atoms. Reviews of Modern Physics, 83(4):1523, 2011.
- [11] Chiara d’Errico, Matteo Zaccanti, Marco Fattori, Giacomo Roati, Massimo Inguscio, Giovanni Modugno, and Andrea Simoni. Feshbach resonances in ultracold 39k. New Journal of Physics, 9(7):223, 2007.
- [12] Richard J Fletcher, Raphael Lopes, Jay Man, Nir Navon, Robert P Smith, Martin W Zwierlein, and Zoran Hadzibabic. Two- and three-body contacts in the unitary bose gas. Science, 355(6323):377–380, 2017.